Mechanics Research Communications. Year	Publication Office: Elsevier UK
Editor-in-Chief: A. Rosato New Jersey Institute of Technology, Newark, New Jersey, USA Anthony.Rosato@njit.edu	

Pantographic Metamaterials Show Atypical Poynting Effect Reversal

Anil Misra[1,3,5*] Tomasz Lekszycki[2], Ivan Giorgio[3,4,5], Gregor Ganzosch[6], Wolfgang H. Müller[6], Francesco dell'Isola[3,4,5]

[1]*Civil, Environmental and Architectural Engineering Department University of Kansas, 1530 W. 15th Street, Learned Hall, Lawrence, KS 66045-7609, USA,*
[2]*Faculty of Engineering Production, Warsaw University of Technology, Warsaw, Poland,*
[3]*International Research Center for Mathematics & Mechanics of Complex Systems (M&MoCS), Università dell'Aquila, Italy,*
[4] *Università di Roma "La Sapienza", Italy,*
[5]*Research Institute for Mechanics, National Research Lobachevsky State University of Nizhni Novgorod, Russia,*
[6]*Institute for Mechanics, TU Berlin, Germany*

*Corresponding author amisra@ku.edu
Tel.:+1-785-864-1750; fax: +1-785-864-5631]
Accepted: xxxxxx., 2018.

Abstract

In an analysis presented in 1909, Poynting (page 546 of[1]) had shown that for finite elastic deformations, the lines of greatest extension and contraction are inclined to the diagonals of the rhombus into which a square is sheared. The implication of this finding was that when slender structures are twisted, they undergo elongation as experimentally verified by Poynting's measurements with wires[1]. While many theoretical analyses have shown the possibility of Poynting and reverse (inverse) Poynting effect [2-7], measurements of such effects are rather sparse[8-11]. We present here measurements of a highly nonlinear Poynting effect, including its reversal from positive to negative (elongation to compression) direction during torsion. Such atypical behavior is exhibited by a rather exceptional material system that has a pantographic internal structure. For this material system, the classical Cauchy-type continuum model fails and a 2nd gradient continuum model is necessary to describe many of its deformation behaviors.

Keywords: Poynting effect; pantograph; second gradient continua; torsion; metamaterials

1. Introduction

The Poynting effect under torsion can be detected as either elongation, shortening or volume change of the sample, or as a measured axial reaction force in the case the sample is prevented from elongation or shortening. Since the original work of Poynting, a positive (elongation) effect under torsion have been observed for elastomers[8, 11] as well as for certain gels[10]. In contrast to that, recent measurements with fiber impregnated semi-flexible biopolymer gels have shown a negative (compressional) Poynting effect[9]. Volume changes under quasi-static torsional shearing have also been observed in glasses[12] and are widely known in granular materials[13, 14], however, the phenomena in glasses and most granular materials are typically due to inelastic (irreversible) deformations and therefore different from the classical Poynting effect. From the viewpoint of theoretical analysis, the Poynting effect has been attributed to nonlinear effects of finite strain elasticity. Utilizing Mooney's form of nonlinear elastic constitutive law, the normal force to prevent extension of a right cylinder has been shown to vary with the square of the torsional twist for small strains[11]. For large strains, this relationship becomes nonlinear[7]. More recent analysis using a 2nd order nonlinear elastic model has shown the possibility of nonlinear inverse Poynting effect with a jump instability[5]. Theoretical analyses have also shown that for particular fiber reinforced materials that exhibit transverse isotropy, the direction of the Poynting effect under torsion can evolve from

the positive to the negative under large deformations[3, 15]. However, such effects have not been measured to our knowledge even in fiber reinforced materials. Remarkably, our recent torsion experiments with 2D plates composed of pantographic lattice structures show a highly nonlinear Poynting effect in which the measured reaction evolves from tensile to compressive.

2. Pantographic Metamaterials

Material systems with pantographic lattice structures are characterized by two families of orthogonal equally spaced beams interconnected via cylindrical pivots as shown in Figure 1. These structures, realized by using standard devices in additive (3D) printing, can be described as multiscale material systems. The elastic pivots interconnecting the beams may have diameters ranging from 0.6 mm and height 1.0 mm onwards, the constituting beams may have sections whose dimensions may range from 0.6 mm onwards and the distance between pivots may range from 2.0 to 20.0 mm. As the resolution of the manufacturing techniques improves, such structures could be realized at micro-scales with millions of basic building blocks. Clearly, the investigated pantographic structure is preconceived and may not appear ordinarily in materials formed by currently extant manufacturing or natural processes. Such considerations could give rise to the perpetual need for distinction between structure and material. However, it is now well-accepted that the response of material system at a certain length-scale (typically termed macroscopic) is affected by the underlying deformation mechanisms, energy distributions and structures at smaller scales. In this regard materials formed from particle precursors (such as geomaterials), show clear manifestations of grain-scale mechanisms in their behaviors at scales comprising millions of grains as shown by their wave dispersion and micromorphic nature[16, 17], and atypical atomic-level deformation mechanisms can even be observed in complex crystalline material systems[18]. Thus, a material system may be ordained as one which can be composed by repeatedly stacking in space a building block of certain length scale, which in our case is the primitive lattice square formed by the orthogonal beams connected by pivots.

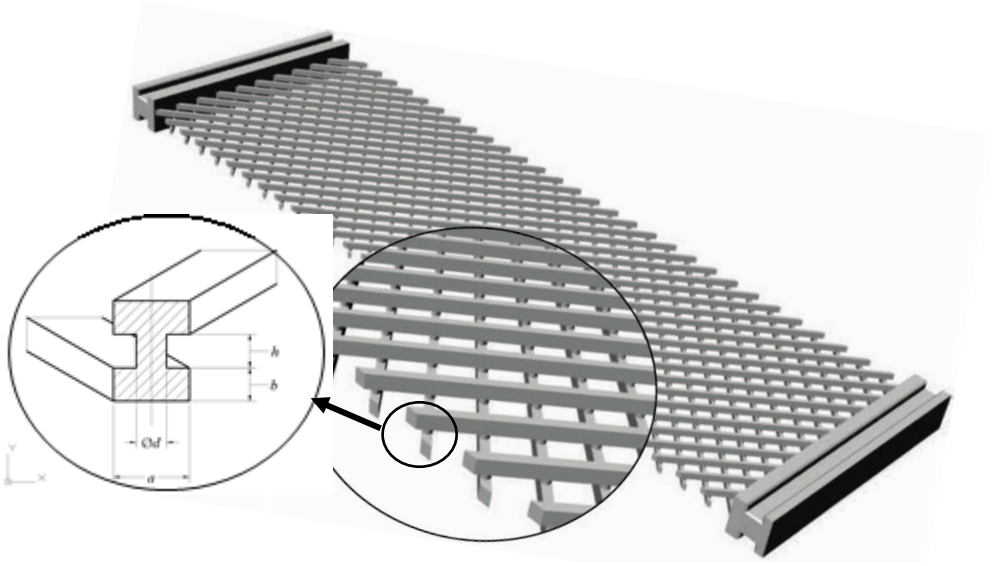

Figure 1- Schematic of continuum material point, P, with its granular microstructure and the coordinate systems x and x'

3. Specimen Fabrication and Torsion Tests

Pantographic lattice specimens with 9 different internal geometries but equal volumetric mass density were fabricated using polyamide as the precursor material. A 3D computer generated model in CAD software SolidWorks (Dassault Systèmes SolidWorks Corporation, Waltham, MA, USA) was used to design the layout of the pantographic lattice specimens. The physical specimens were realized in 3D printer (P 100, EOS GmbH, Munich, Germany) which uses a laser sintering technology to build-up components layer-by-layer from fine powders. Polyamide powder of average grain size 56 μm was used as the precursor material for these specimen. Nine types of specimens with different internal geometries, but equal volumetric mass density, were printed. The overall dimension of all the specimens was 210 mm x 70 mm. Table 1 gives the dimensions of the beam cross-section, beam spacing, pivot diameter and heights and the stiffness order. The beam and pivot dimensions were varied in these specimens with the aim to understand the mechanisms and effect of the substructure properties on the overall behavior of these material systems.

These specimens were then tested under torsion. A Zwick Z010 testing device controlled by the software TestExpert was used for the torsion tests. A schematic of the loading and measurement device is shown in Figure 2. The resultant applied axial force was measured by a load cell Zwick-Serie XforceK that is attached to the device. The force transducer is able to record axial forces in the range of ±10 kN. The accuracy of the force transducer in the range ±20 N was determined to be 0.1% by calibration with standardized weights. The

vertical/axial displacement was set to zero. For the torsion measurement, a torque sensor (Zwick-Serie M) was used at the fixed bottom of the traverse. The specimen torsion was induced via traction drive on the top of the mounting at the rate 1°/min. The torque sensor is able to record moments up to 100 Nm. In addition, the non-invasive optical measurement device Q-400 (Dantec Dynamics GmbH, Ulm, Germany) was installed to record the state of three dimensional deformation. During the deformation process, pictures have been taken every 2 seconds by means of the aforementioned commercial DIC camera system with a resolution of 1600 x 1200 pixels.

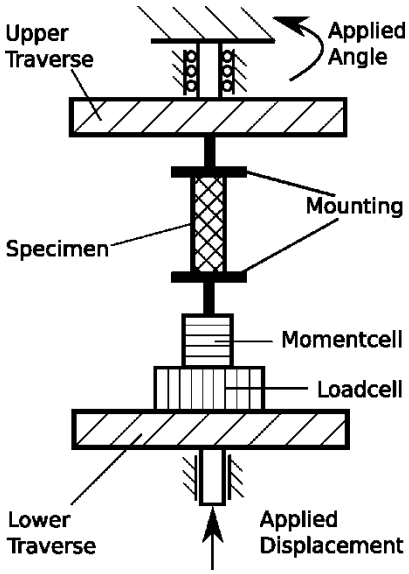

Figure 2- Schematic of the loading and measurement device*'*

4. Results and Discussion

Figure 3 gives the snapshots of a torqued specimen at various twist angles. The elongation or shortening in the axial direction of the specimens is restricted during the test and the corresponding reaction force is measured. Figure 4(A) gives the axial reaction force (Poynting effect) as a function of the square of the normalized twist angle, θ, for the hardening part of the torque-twist behavior shown in Figure 4(B). In the twist angles range shown in the figures, the specimen exhibits no damage and the behavior remains recoverable. In contrast to the observed nonlinear behavior for the tested specimens, the classical Poynting effect is known to show a linear relationship of axial reaction force with the square of the twist angle. More significantly, we observe that for some specimen the positive Poynting effect reverses and, subsequently, becomes negative as the twist progresses as seen for specimens 1 through 5 (shown separately in the box for clarity). And notably the twist angle at the reversal and transition from positive to negative Poynting effect varies with internal geometric parameters.

During the twist of the specimen, two deformation mechanisms and their energetic contributions control the behavior of this material system. First, the beams forming the lattice undergo bending to wrap around the specimen's twist axis into 'helical'-shapes as seen in Figure 3; and second, the two orthogonal family of beams rotate relative to each other as the interconnecting pivot is micro-twisted producing macro-shear. The 'helix' angle of the deformed beams is affected by the relation between energies associated with different deformation modes. These deformation energies depend upon the geometrical and stiffness parameters of the pantographic lattice, which include the distance between pivots (lattice cell size), the dimensions of beam cross-section, the pivot diameter and height (details in the Table 1). The consequence of the helical beam deformation is that the square lattice cells shear into rhomboid shapes with major axes aligned either primarily to the axis of rotation resulting in a tendency of overall specimen elongation or primarily orthogonal to the axis of rotation resulting in a tendency of overall specimen shortening. Here the insight given to us by the original consideration by Poynting is remarkable.

Clearly, the genesis of the observed atypical nonlinear Poynting phenomena lies in the relation between energies of deformation modes which is influenced by the relative flexural stiffness of the beams and shear stiffness of the pivots in our pantographic structure. This mechanical intuition, reinforced by the geometrically based considerations by Poynting, are made precise by the numerical simulations we have performed using generalized plate theory proposed in[19]. Figure 4(C) gives the stiffness order of the 9 specimen calculated as the ratio of the beam flexural stiffness to pivot shear normalized by the stiffness ratio of specimen 5. The indication is that for the pantographic lattice structures formed of relatively soft beams and stiff pivots, a positive Poynting effect dominates. In these cases, the relative rotations between the connected beams is suppressed while the softer beams bend easily resulting in a

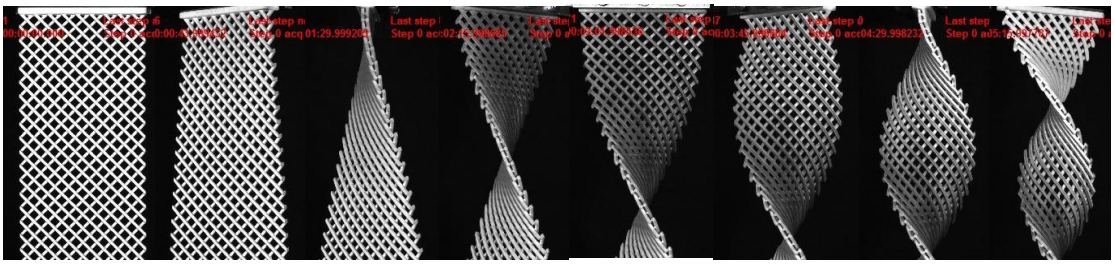

Figure 3- Snapshots of specimen 3 under torsion at twist angles θ = 0, 45°, 90°, 135°, 180°, 225°, 270°, and 315°, respectively.

larger 'helix' angle. As a consequence, the major axis of the deformed rhomboid cell is aligned to the axis of rotation and the structure has a tendency to elongate. Since the elongation is prevented in our experiment, a positive reaction force is measured as is the case of specimens 6 to 9. On the other hand, for the case of stiff beams and soft pivots, the beams resist bending while the relative rotation between the two families of beams is easier as the pivots are easily sheared resulting in a relatively smaller 'helix' angle. Therefore in this case, the major axis of the deformed rhomboid shape becomes closer to the direction orthogonal to the axis of twist leading to shortening of the specimen. Thus a negative reaction force would be measured as in the case of specimens 1 and 2.

pivot geometry, and therefore, the same shear stiffness, however, the beam stiffness for specimen 3 is almost 6 times larger. Remarkably, this large difference in stiffness is achieved by increasing the cross-section area by 2.56 times. While the volume of primitive elements in these material systems scale by the square of their characteristic dimension, the stiffness scales by a power of 4. Thus, small changes in micro-dimensions/mechanisms have the potential to greatly alter the overall behavior.

For efficient mathematical description and optimization of these multi-scalar material systems specific models must be formulated at every scale. At the macro length scale of our material system, a particular form of second gradient

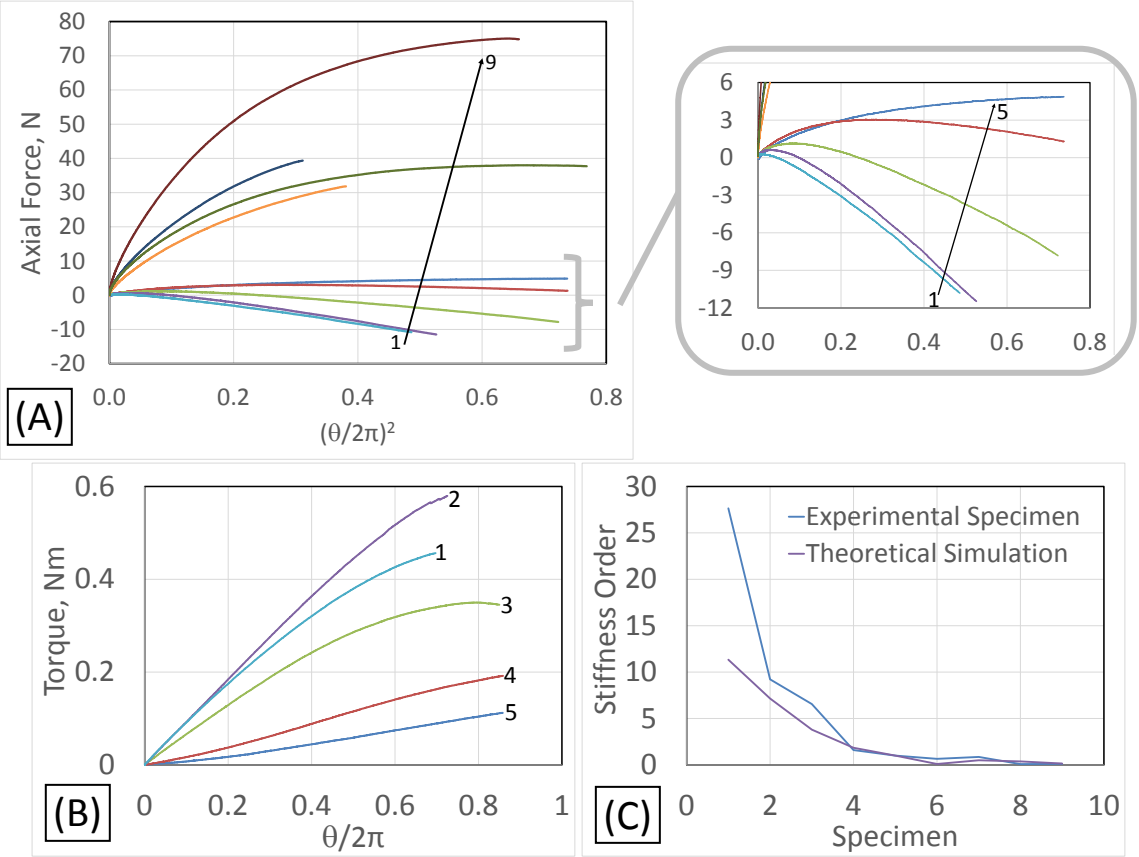

Figure 4- (A) Measured Poynting effect for the 9 specimens. (B) Torque-twist behavior for the specimens 1 through 5 that exhibited widely contrasting Poynting behavior including reversal from positive to negative Poynting effect. It is notable that the volumetric mass density had negligible variation among specimens 1-5. (C) Stiffness order of the 9 specimens calculated by normalizing with the stiffness ratio of specimen 5.

For the intermediate cases, the behavior is complex as exemplified by specimens 3 to 5. In these cases, the two deformation mechanisms compete as the overall twist deformation progresses. In the early part of the twist, the flexural deformation energy of beams appears to dominate while in the later part the shear energy of pivots dominates. The orthogonal family of beams first bend resulting in a tendency for overall specimen elongation and a positive Poynting effect. As the twist angle increases, the pivot shear deformation becomes dominant. The result is that the Poynting effect first reduces, then reverses and finally becomes negative. Specimens 3 and 5 give a clear demonstration of the two competing mechanisms. Both these specimens have the same

continuum model is most suitable[19]. The need of enhanced continuum models are being increasingly recognized for describing unusual material behavior [20, 21]. In the approach implemented here, the pantographic lattice is modeled as a 2D continuum with a suitable internal structure which is made latent by imposing certain internal constraints[19]. In this approach, the kinematic variables of the lattice are expressed in terms of the coarse descriptors of deformations relevant to 2D generalized plate continua. The strain energy function of the 2D body is then constructed in terms of the coarse descriptors and results in the introduction of five stiffness constants for the continuum body, which are related to the elongation Ke, twisting Kt, normal and geodesic bending, Kn and Kg, of the

beam latent in the REV, as well as the shear stiffness Ks of the pivots latent in the REV (see [22] for identification of the continuum constants in terms of the beams and pivot properties). The resultant 2nd gradient model has been solved using COMSOL Multiphysics finite-element software for obtaining the theoretical predictions in Figure 5. Table 2 gives the stiffness parameters used to mimic the behavior of specimen 1 through 9 by changing the stiffness order. Figure 5 shows that the 2nd gradient model particularly conceived for the investigated material system also predicts the observed Poynting effect reversal reported in this letter. This heuristic continuum model has a representation of bending and shear stiffness relevant to our material system although the direct connection to the beam and pivot stiffnesses have not been made. Remarkably the predictions follow similar trend of stiffness order as the experiments as seen from Figure 4(C) demonstrating that such metamaterial systems can indeed be tuned. The study has demonstrated that materials with nonlinear reversible Poynting effect can indeed be realized. The ability to harness the Poynting effect is critical for the design of soft materials and biological tissues functioning under large deformations [5, 9, 10].

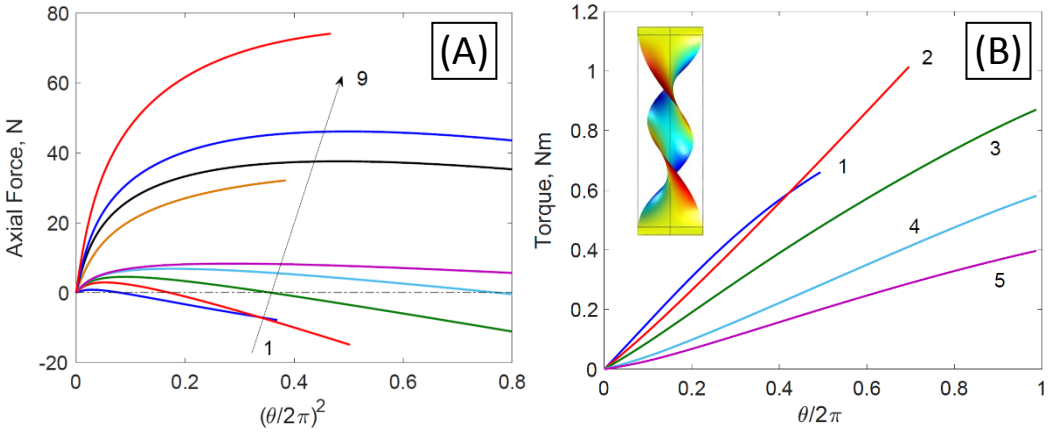

Figure 5- (A) Predicted Poynting effect utilizing a 2nd gradient continuum model. (B) Predicted torque-twist behavior for the specimens 1 through 5 that exhibited widely contrasting Poynting behavior including reversal from positive to negative Poynting effect. Inset shows an example simulated deformed configuration at 360°.

Acknowledgements. AM is supported by the National Science Foundation (NSF) under CMMI-1727433. FD, IG and AM are also supported by a grant from the Government of the Russian Federation (No. 14.Y26.31.0031).

References

[1] J. Poynting, On pressure perpendicular to the shear planes in finite pure shears, and on the lengthening of loaded wires when twisted, Proceedings of the Royal Society of London. Series A, Containing Papers of a Mathematical and Physical Character 82(557) (1909) 546-559.

[2] F. Dell'Isola, G.C. Ruta, R.C. Batra, Generalized Poynting effects in predeformed prismatic bars, Journal of elasticity 50(2) (1998) 181-196.

[3] C. Horgan, J. Murphy, Poynting and reverse Poynting effects in soft materials, Soft Matter 13(28) (2017) 4916-4923.

[4] D. Wang, M.S. Wu, Poynting and axial force–twist effects in nonlinear elastic mono- and bi-layered cylinders: Torsion, axial and combined loadings, International Journal of Solids and Structures 51(5) (2014) 1003-1019.

[5] M. Wu, H. Kirchner, Nonlinear elasticity modeling of biogels, Journal of the Mechanics and Physics of Solids 58(3) (2010) 300-310.

[6] O. Bruhns, H. Xiao, A. Meyers, Hencky's elasticity model with the logarithmic strain measure: a study on Poynting effect and stress response in torsion of tubes and rods, Archives of Mechanics 52(4-5) (2000) 489-509.

[7] E. Billington, The Poynting effect, Acta mechanica 58(1) (1986) 19-31.

[8] A. Freudenthal, M. Ronay, Second order effects in dissipative media, Proceedings of the Royal Society of London A: Mathematical, Physical and Engineering Sciences 292(1428) (1966) 14-50.

[9] P.A. Janmey, M.E. McCormick, S. Rammensee, J.L. Leight, P.C. Georges, F.C. MacKintosh, Negative normal stress in semiflexible biopolymer gels, Nature materials 6(1) (2007) 48-51.

[10] S. Misra, K. Ramesh, A.M. Okamura, Modelling of non-linear elastic tissues for surgical simulation, Computer methods in biomechanics and biomedical engineering 13(6) (2010) 811-818.

[11] R.S. Rivlin, D. Saunders, Large elastic deformations of isotropic materials. VII. Experiments on the deformation of rubber, Philosophical Transactions of the Royal Society of London A: Mathematical, Physical and Engineering Sciences 243(865) (1951) 251-288.

[12] R.S. Duran, G.B. McKenna, A torsional dilatometer for volume change measurements on deformed glasses: Instrument description and measurements on equilibrated glasses, Journal of Rheology 34(6) (1990) 813-839.

[13] O. Reynolds, LVII. On the dilatancy of media composed of rigid particles in contact. With experimental illustrations, The London, Edinburgh, and Dublin Philosophical Magazine and Journal of Science 20(127) (1885) 469-481.

[14] F. Tatsuoka, M. Muramatsu, T. Sasaki, Cyclic undrained stress-strain behavior of dense sands by torsional simple shear test, Soils and Foundations 22(2) (1982) 55-70.

[15] C.O. Horgan, J.G. Murphy, Reverse Poynting effects in the torsion of soft biomaterials, Journal of Elasticity 118(2) (2015) 127-140.

[16] A. Misra, P. Poorsolhjouy, Granular micromechanics based micromorphic model predicts frequency band gaps, Continuum Mechanics and Thermodynamics 28(1-2) (2016) 215.

[17] A. Misra, P. Poorsolhjouy, Grain-and macro-scale kinematics for granular micromechanics based small deformation micromorphic continuum model, Mechanics Research Communications 81 (2017) 1-6.

[18] A. Misra, W. Ching, Theoretical nonlinear response of complex single crystal under multi-axial tensile loading, Scientific reports 3 (2013).

[19] I. Giorgio, N. Rizzi, E. Turco, Continuum modelling of pantographic sheets for out-of-plane bifurcation and vibrational analysis, Proc. R. Soc. A 473(2207) (2017) 20170636.

[20] T. Frenzel, M. Kadic, M. Wegener, Three-dimensional mechanical metamaterials with a twist, Science 358(6366) (2017) 1072-1074.

[21] E. Turco, I. Giorgio, A. Misra, F. Dell'Isola, King post truss as a motif for internal structure of (meta) material with controlled elastic properties, Royal Society open science 4(10) (2017) 171153.

[22] L. Placidi, U. Andreaus, A. Della Corte, T. Lekszycki, Gedanken experiments for the determination of two-dimensional linear second gradient elasticity coefficients, Zeitschrift für angewandte Mathematik und Physik 66(6) (2015) 3699-3725.

Table 1: Beam and pivot geometrical properties (mm) and stiffness order.

Type	a	b	l	d	h	Ixx	Iyy	J/h	Ixx/J/h	Stiffness order
1	2.25	1.6	6	0.9	3	9.22	18.23	0.22	42.14	27.65
2	2.25	1.6	6	0.9	1	9.22	18.23	0.66	14.05	9.22
3	1.6	1.6	5.5	0.9	1	6.55	6.55	0.66	9.99	6.55
4	1.6	1	5	0.9	1	1.60	4.10	0.66	2.44	1.60
5	1	1	4	0.9	1	1.00	1.00	0.66	1.52	1.00
6	0.6	0.6	1.75	0.6	1	0.13	0.13	0.13	1.00	0.66
7	0.8	1.8	4.5	1.3	0.8	4.67	0.92	3.57	1.31	0.86
8	1.6	0.9	4.5	1.7	1	1.17	3.69	8.35	0.14	0.09
9	0.7	1.7	4.5	1.7	0.4	3.44	0.58	20.88	0.16	0.11

Table 2: Stiffness parameters for the continuum model.

Type	Ke, N/m	Kg, Nm	Kn, Nm	Kt, Nm	Ks, N/m	Stiffness Order
1	139000	0.06	0.35	0.15	0.37	11.34
2	581800	0.25	0.27	0.19	0.61	7.16
3	413800	0.09	0.19	0.10	0.66	3.80
4	258600	0.06	0.09	0.05	0.66	1.84
5	161600	0.01	0.05	0.03	0.66	1.00
6	58180	0.00	0.02	0.01	1.96	0.10
7	232700	0.01	0.10	0.04	2.40	0.50
8	232700	0.05	0.07	0.05	2.81	0.38
9	192330	0.01	0.05	0.02	4.39	0.15